Flow Measurement and Instrumentation 46 (2015) 58–65

Contents lists available at ScienceDirect

Flow Measurement and Instrumentation

journal homepage: www.elsevier.com/locate/flowmeasinst

Insertion calorimetric flowmeter for liquids with multiple temperature sensors to improve measurement by redundancy

Alberto J. Molina *, Félix Biscarri, Miguel Ángel Leal, Manuel Merino

Department of Electronic Technology, University of Sevilla, Escuela Politécnica Superior, Virgen de África n. 7, 41011 Sevilla, Spain

ARTICLE INFO

Article history:
Received 22 June 2015
Received in revised form
27 August 2015
Accepted 28 September 2015
Available online 24 October 2015

Keywords:
Thermal
Flow
Measurement
Redundancy
Calorimetric
Sensor
Water

ABSTRACT

In this paper a thermal flowmeter based on the calorimetric principle is reported and analytically modeled. The flow is measured without using any kind of laminar or bypass elements and it has been tested for laminar, transitional and turbulent flow patterns. It contains four temperature sensors. Three of them are placed downstream and the fourth upstream. Results showed that the model qualitatively describes the relationship between temperature and mean velocity in laminar flows. The meter accuracy is increased by combining the flow estimations given by three downstream sensors (redundancy of measurements) and by continuously correcting the dependency that the calorimetric method shows on fluid temperature. Experimental results, using water as fluid, make the accuracy rate of the instrument equal to ± 0.7% FS in a range between 0.5 L/min and 19 L/min, which is not a usual range for thermal flowmeters in liquids. Finally, an algorithm to prevent the probe from damaging in practical implementations is shown.

1. Introduction

Thermal flowmeters are widely used nowadays in industrial processes and they can be classified according to the measurement principle: hot-wire, calorimetric and time-of-flight (TOF) [1–3]. *Hot-wire* (film-wire) *sensors* measure the effect of a fluid flowing around a hot body. According to the physical parameter that is kept constant, hot-wire flowmeters can be classified as follows: constant temperature, constant current or constant power. In constant temperature mode the main body is heated up, until it reaches a specific temperature, and it is maintained on it. The flow is detected, and quantified, by measuring the power that is needed to keep the main body temperature. In the other modes, the flow is measured by any electrical signal that reflects the cooling effect that the flow causes to the hot body. *Calorimetric sensors* [4–7] are based on measuring temperature shifts around a heater. In a situation of zero flow, the temperature profile is symmetrical with respect to the heater. A temperature sensor placed downstream away from the heater will register the same value that another one placed at the same distance from the heater but upstream. Therefore, the temperature difference between them equals zero. If the flow is not zero, the temperature profile shifts by transport in the flow direction, so the values registered by the two temperature sensors will be different. *Time-of-flight* sensors measure how long a heat pulse takes to get to a temperature sensor placed downstream. This kind of flowmeter can be implemented by putting heat marks into the fluid or by continuously driving the heater with an ac signal and measuring the phase shift at the position of the temperature sensor. Most commercial thermal flowmeters are based, mainly, on hot-wire principles but in the scientific literature it is also common to find ones based on calorimetry [4–7], or using a combination of different thermal principles, for instance: calorimetric and hotwire [8,9] or TOF and calorimetric [10], etc.

The kind of fluid whose flow is measured is important in thermal flowmeters. Most commercial devices are developed for gases like air, O_2, CO_2, etc. and very few vendors offer hot-wire-based flowmeter for liquids. Researchers have reported thermal flowmeters for liquids [11] but with low measuring range (between some nL/min [12], 500 μL/min [13] and 500 mL/min [14]). A wider range (up to 0.25 L/min) has been also reported [15,16] but, in these cases, the proposal flowmeters were based on the hot-wire method.

With regard to the calorimetric probes, almost all commercial meters use bypass and also include laminar elements inserted into the main flow. An insertion calorimetric probe was proposed in this work, thus laminar element and the bypass pipe are avoided. This flowmeter has been tested using liquid (water) instead of gases and the test flow range yields between 0.4 L/min and 19 L/min, which overcomes most commercial calorimetric flowmeters with a good turndown ratio of 46:1. The selected flow range makes Reynolds number change from 454 up to 19745, so, laminar,

* Corresponding author. Fax: +34 954552764.
E-mail address: almolina@us.es (A.J. Molina).

http://dx.doi.org/10.1016/j.flowmeasinst.2015.09.008
0955-5986/

transitional and turbulent flows are all included in the experimental test. Moreover, three temperature sensors are placed downstream to combine multiple measurements into one estimation of flow with a lower error.

The rest of the paper is organized as follows: Sections 2 and 3 show the structure of the proposal sensor and the analytical model respectively. Section 4 shows the acquisition circuit, transduction equations and the fluid temperature compensation method. Sections 5, 6 and 7 show the experimental results, the flowmeter accuracy with its operational modes and the conclusions respectively.

2. Flowmeter sensor

The experimental probe, shown in Fig. 1, is made of a central heater and four 1 kΩ class B Pt1000 temperature sensors.

Three of them (T_n, $n=1,2,3$) are placed downstream, whereas the fourth one (T_r), or reference sensor, is located upstream. The heater consists of an etched-foil resistive heating element, placed between T_r and T_1, with a resistance value equal to 13 Ω and it might dissipate up to 3 W.

The probe is fully covered with a water-resistant Kapton isolation layer and stuck on a 2-mm-thick FR4 substrate that gives it stiffness. The experimental probe is inserted into the pipe, splitting its internal room into two almost semicylindrical spaces, and with temperature sensors at the axial position of the pipe. The probe is inserted in the center of the pipe with a distance equal to 10 cm from the probe to any end of the pipe (Fig. 2). Connection pads for sensors and heater remain out of the pipe and the space between the external part of the probe and the pipe were sealed to avoid the leakage of the fluid.

3. Analytical model

Applying the energy balance to a slice of a control volume (CV) placed over the probe, as it is shown in Fig. 3, we obtained an analytical model of the heat transport phenomena. In steady state, the energy per unit time entering the control volume in any direction (x, y, z) is equal to the output one. The main heat transport phenomena happen in the x-direction, where there are advection and diffusion effects quantified by Eqs. (1) and (2). The parameters ρ, c_p, v, K are the density, heat capacity, velocity and thermal conductivity of the fluid respectively. Some geometric parameters are the width of the heater, w, and the height of the CV, $\delta(x)$, which, in turn, is dependent on x.

$$[q_{adv}(x) - q_{adv}(x+dx)]w\delta(x) = [T(x) - T(x+dx)]\rho c_p v w\delta(x) = -\rho c_p v \frac{dT}{dx} w\delta(x)\,dx \tag{1}$$

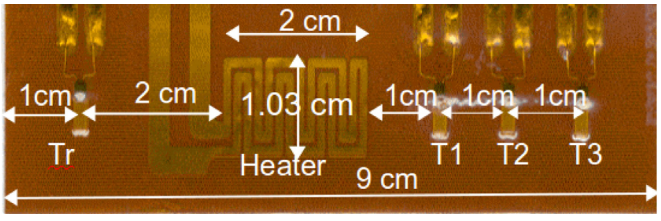

Fig. 1. Experimental flowmeter probe. It contains a heater and four temperature rtd-type sensors, three placed downstream and an upstream one acting as a reference and for fluid temperature measurement.

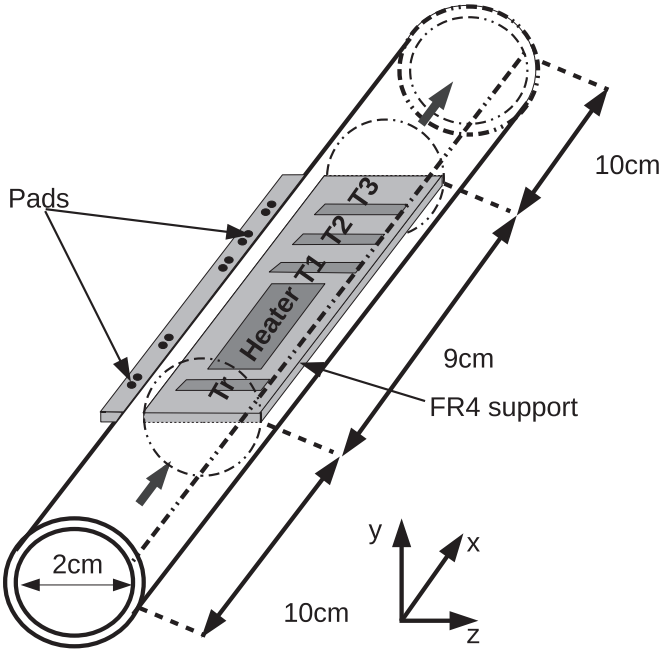

Fig. 2. Flowmeter probe inside the pipe.

$$(q_{dif}(x) - q_{dif}(x+dx))w\delta(x) = K\left[-\frac{dT(x)}{dx} + \frac{dT(x+dx)}{dx}\right]w\delta(x) = K\frac{d^2T}{dx^2}w\delta(x)\,dx \tag{2}$$

In the y-direction there is no heat flow through the top side of the control volume. This is because its height, $\delta(x)$, has been chosen equal to the height of the thermal boundary layer, wherein the heat transport phenomena take place. At the bottom surface, the control volume loses heat by diffusion through the FR4 substrate towards the fluid which is at an ambient temperature. Additionally, whether the control volume is over the heater it receives energy from it. We made the assumption that the power was completely transferred to the fluid, like whether the heater would have been placed into the CV. In Eq. (4), $2L$ is the length of the heater, P the power and $p_{2L}(x)$ is a step function which returns 1 if $-L \le x \le L$ and 0 otherwise. Note the height of the thermal boundary layer is also a function of position, x, increasing as x does. In Eq. (3) the parameters h_s and K_s are the height and the heat conductivity of the FR4 substrate respectively.

$$q_s = K_s\frac{T(x)}{h_s}w\,dx = K_s\frac{T(x)}{h_s\delta(x)}w\delta(x)\,dx \tag{3}$$

$$q_h = \frac{P}{2Lw\delta(x)}p_{2L}(x)w\delta(x)\,dx \tag{4}$$

Combining Eqs. (1)–(4) and assuming that the heat transfer in the z-direction was negligible we obtained the following equation:

$$K\frac{d^2T}{dx^2} - \rho c_p v\frac{dT}{dx} - K_s\frac{T}{h_s\delta(x)} + \frac{Pp_{2L}(x)}{2Lw\delta(x)} = 0 \tag{5}$$

To ease the analytical solution of the above equation the function $\delta(x)$ was substituted by the constant $\bar{\delta}$ or average height of the thermal boundary layer. The limits of integration were set from

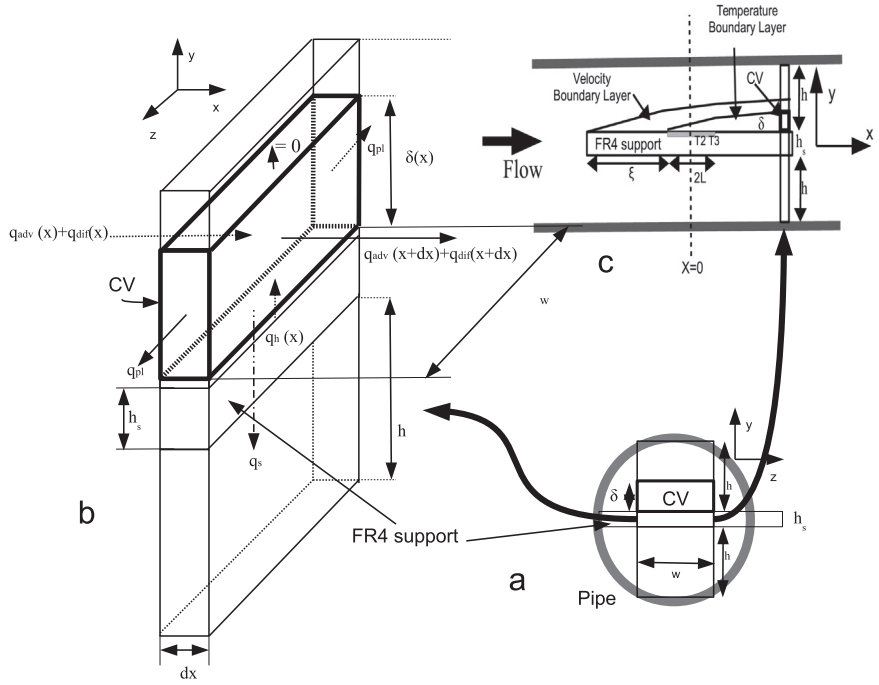

Fig. 3. (a) Cross section of the pipe. The FR4 substrate is placed in the middle and the CV is over it. (b) Details of energy balance in the CV. Read text for details. (c) Longitudinal section of the pipe. Thermal and velocity boundary layers are plotted. The height of the thermal boundary layer defines the height of the CV which has been drawn at the end of the substrate for clarity.

Table 1
Numerical results obtained by applying real physical conditions in Eqs. (6), (11), and (12). The appendix contains the physical values. The heater power was set to $P=2.7$ W and the mean velocities inside the pipe have been chosen similar to the experimentation.

n	v (cm/s)	Re	$\gamma_2 \times 10^2$ (cm^{-1})	$\gamma_1 \times 10^{-3}$ (cm^{-1})	$\bar{\delta}$ (cm)	T_o (°C)
1	2.3	455	−2.13	1.64	0.27	1.00
2	4	794	−1.61	2.86	0.21	0.76
3	6.9	1377	−1.22	4.97	0.16	0.58
4	9.8	1959	−1.02	7.07	0.13	0.48
5	11.5	2298	−0.95	8.29	0.12	0.45
6	18.8	3748	−0.94	13.53	0.08	0.44
7	23.9	4765	−0.22	17.20	0.25	0.10
8	32.8	6544	−0.17	23.63	0.23	0.08
9	47.7	9530	−0.12	34.41	0.22	0.06
10	98.1	19,590	−0.07	70.74	0.19	0.03

$x = -L$, or the initial position of the thermal layer, up to the position of the furthest downstream sensor, x_3.

$$\bar{\delta} = \frac{1}{L + x_3} \int_{-L}^{x_3} \delta(x)\, dx \tag{6}$$

The height $\delta(x)$ of the thermal boundary layer depends on the type of flow. For laminar ones $\delta(x) = \delta_{lam}(x)$ as it is shown in Eq. (7), where Pr is Prandtl's number. For turbulent flows the expression is given by Eq. (8). In both formulas, ξ is the distance between the heater and the border of the substrate, and Reynolds' local number Re_x is given by Eq. (9) where μ is the dynamic viscosity of the fluid.

$$\delta_{lam}(x) = 5x\left[1 - \left(\frac{\xi}{x}\right)^{3/4}\right]^{1/3} Re_x^{-1/2} Pr^{-1/3} \tag{7}$$

$$\delta_{tur}(x) = 0.343x\left[1 - \left(\frac{\xi}{x}\right)^{9/10}\right]^{1/9} Re_x^{-1/5} \tag{8}$$

$$Re_x = \frac{\rho v x}{\mu} \tag{9}$$

In [17,18,6] similar differential equations have been developed and solved with other geometries and boundary conditions. In [17,18] the authors assumed that the temperature along the heater was constant. Following a similar approach, where $T(x) = 0$ for $x \to \pm\infty$ and the heater temperature, T_0, does not depend on x, the solution of Eq. (5) is

$$T(x) = \begin{cases} T_0 e^{\gamma_2(x-L)}, & x > L \\ T_0 e^{\gamma_1(x+L)}, & x < -L \\ T_0, & -L \le x \le L \end{cases} \tag{10}$$

$$\gamma_{1,2} = \frac{\rho c_p}{2K}\left(v \pm \sqrt{v^2 + \frac{4KK_s}{\rho^2 c_p^2 h_s \bar{\delta}}}\right) \tag{11}$$

$$T_0 = \frac{P}{K_s \frac{2Lw}{h_s} + Kw\bar{\delta}(\gamma_1 - \gamma_2)} \tag{12}$$

Table 1 shows numerical results of some parameters of the model using real physical constants and similar flows used in experimentation. For transitional flows (v_6) the thermal boundary layer thickness was obtained by linear interpolation between the values associated to v_5 and v_7.

Fig. 4 shows several plots of the temperature distribution obtained by applying experimental conditions to above equations. The positions of heater and temperature sensors have been also drawn in abscissas axis. Velocities v_1 and v_4 are associated to laminar flows whereas the other two to turbulent ones. It can be seen that just for low velocities (v_1 for example), the temperature exponentially decays as x increases. For the rest, the temperature is more or less flat, suggesting that there will not be important differences among the temperature that the downstream sensors

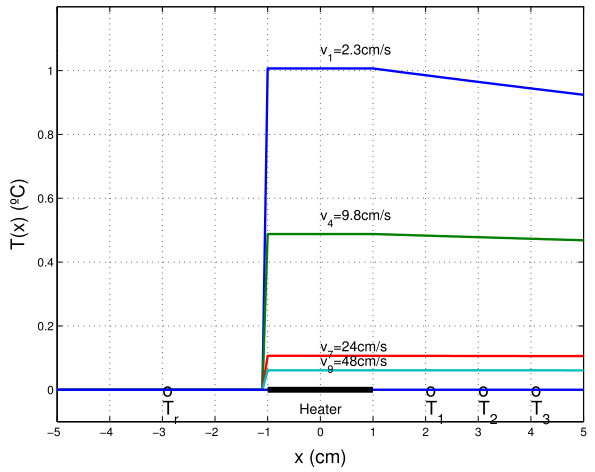

Fig. 4. Temperature distribution along the x-axis for different fluid velocities and flow patterns. The position of temperature sensors and heater are also plotted. Laminar flows are represented by fluid velocities v_1 and v_4, turbulent flows by the two others.

measure and the one the heater reaches.

For the conditions used in experimentation, Eq. (11) can be simplified as $\gamma_1 \approx \rho c_p v/K$ and $\gamma_2 \approx 0$ (see Table 1). This simplification also affects Eq. (12). Its denominator contains two terms. The left one is smaller than the other, so $T_0 \approx P/Kw\bar{\delta}(\gamma_1 - \gamma_2)$, and substituting the simplified γ_1 and γ_2 into it makes $T_0 \approx P/w\rho c_p \bar{\delta} v$. Moreover, $\bar{\delta}$ is dependent on velocity according to Eq. (7) or (8). For laminar flows $\bar{\delta} \propto v^{-0.5}$, so $T_0 \propto v^{-0.5}$ too, whereas for turbulent flows $\bar{\delta} \propto v^{-0.2}$ and hence $T_0 \propto v^{-0.8}$.

4. Acquisition circuit

A simplified analog schematic is shown in Fig. 5. The first stage includes temperature sensor into resistive dividers powered with a 2.5 V voltage reference circuit. The reference sensor is connected to a resistor with a 0.1% tolerance, whereas the resistor dividers of the T_n sensors contain variable resistors in order to calibrate the baseline, or the voltage value for zero flow condition. Voltage coming from the T_r sensor is buffered and used as a reference signal for the signals coming from sensors T_n and for measuring fluid temperature. A second-circuit stage amplifies the bipolar $T_n - T_r$ voltage signal and contains a low-pass filter with a 2 Hz cutoff frequency. The filtered signal is then amplified and biased in order to comply the electrical input range of the ADC. Each channel has been oversampled at 800 Hz/channel and then averaged using an 800-sample window, so four measurements per second are available (fluid temperature and $T_n - T_r$, where $n=1,2,3$) [19].

4.1. Signal amplitude

In the calorimetric method the heater is continuously turned on and the flow is correlated with the temperature difference $T_n - T_r$. As is shown in Fig. 5, the signal voltage from resistors dividers is given by Eq. (13), where V_{ref} is the voltage supply of the bridge, A is the gain of the circuit, R_n for ($n=1,2,3$), and R_r are the resistive values of RTDs, R_4 and R_5 are the resistances placed in the same branch of R_n and R_r respectively, and T_n (for $n=1,2,3$), T_r are the fluid temperature at position of the sensors. Notice that R_n and R_r are temperature dependent, so they appear in the equation as a function of fluid temperature at the position of the sensor.

$$V_n = V_{ref} A \frac{R_n(T_n)R_5 - R_r(T_r)R_4}{[R_n(T_n) + R_4][R_r(T_r) + R_5]} \tag{13}$$

The output signal, V_n, is driven to zero by adjusting R_4 during the calibration process, which takes place when the heater is off. In such a situation, all sensors detect the same temperature, the fluid temperature, T_f so $T_n = T_r = T_f$. Adjusting R_4, as in Eq. (14) shows, makes V_n not depend on T_f so V_n will go on being zero even though the fluid temperature changes.

$$R_4 = \frac{R_5 R_n}{R_r} \tag{14}$$

After the calibration process, the heater is then turned on. From this moment, any change on V_n is due to heat transport phenomena that makes local temperature at downstream sensors positions rise. Let δT_n be the difference of temperature between sensor n and the reference one.

$$\delta T_n = T_n - T_r \tag{15}$$

This incremental temperature depends on flow and distance between the sensor and the heater. For RTD resistors, the resistive value is approximately linear with temperature, $R_n = R_0(1 + \alpha T_n)$. So Eq. (13) can be written as in the following equation:

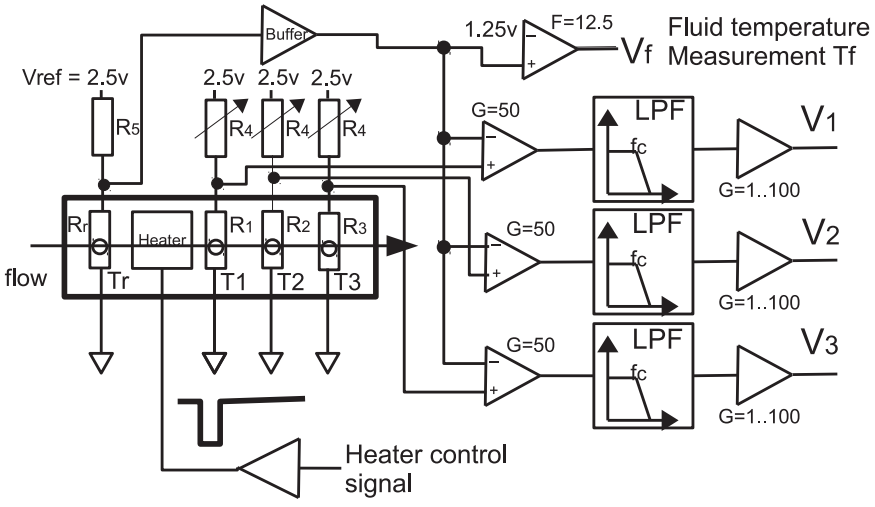

Fig. 5. Data acquisition circuit. Three out of four outputs are for flow measurement. Fourth output is for measuring fluid temperature for further compensation. Each V_n pathway contains amplifiers and a low pass filter.

$$V_n = V_{ref} A \frac{R_0 R_5 \alpha \delta T_n}{\left[R_n(T_f + \delta T_n) + R_4\right]\left[R_r(T_f) + R_5\right]} \tag{16}$$

The sensitivity of V_n is about 2.26 mV/°C for a standard fluid temperature of 25 °C.

4.2. Fluid temperature compensation

Assuming $\delta T_n < T_f$, we can simplify $R_n(T_f + \delta T_n) \approx R_n(T_f)$ and taking into account the zero flow calibration value for the bridge elements, Eq. (14), and substituting it into Eq. (16) then it turns into the following equation:

$$\delta T_n \simeq \frac{V_n}{V_{ref} A} \frac{R_4\left[R_r(T_f) + R_5\right]^2}{R_0 R_5^2 \alpha} \tag{17}$$

As we can see from Eq. (17), the final result depends on fluid temperature. The influence of T_f on the measured signal can be analyzed by just taking derivative to Eq. (17). The result is that the output signal depends on fluid temperature over 0.4%/°C. Therefore, a variation over 10°C on the fluid temperature will produce an error higher than 4% on the output signal, so a compensation mechanism is required. Several techniques for fluid temperature compensating have been published [20,21] but an easy way to achieve this is to measure fluid temperature and put it into Eq. (17). Although fluid temperature measurement will have an error, for instance below 0.5 °C, it will help δT_n dependency on T_f keep lower than 0.2%.

The signal V_f (see Fig. 5) allows the estimation of the fluid temperature T_f based on the signal coming from the upstream sensor in the probe, which is not affected by the heater. Eq. (18) shows the relationship between V_f and the fluid temperature T_f, where F is the amplifier gain set to 12.5. Substituting $R_r(T_f) = R_0(1 + \alpha T_f)$ into Eq. (18) and solving for T_f we obtained Eq. (19) for fluid temperature.

$$V_f = V_{ref} F \left(\frac{R_r(T_f)}{R_r(T_f) + R_5} - \frac{1}{2} \right) \tag{18}$$

$$T_f = \frac{R_5}{R_0 \alpha} \left(\frac{V_{ref} + \frac{2}{F} V_f}{V_{ref} - \frac{2}{F} V_f} \right) - \frac{1}{\alpha} \tag{19}$$

5. Results

Experimentation was carried on using a testbed for setting and measuring the flow of the fluid passing the probe. Ten different flows have been chosen, and an overall of 25 measurements for each one have been carried out in order to know the repeatability of the measurements. Fluid temperature has been measured trial by trial, showing a variation close to 7 °C from the beginning up to the end of a sequence of trials. Eq. (17) was used to compensate such a temperature drift.

Figs. 6 and 7 show the experimental values of δT_n and how they depend on flow and the distance between the downstream sensor and the heater. The temperature δT_n decreases as flow and the heater–sensor distance increase. In laminar flows δT_n follows a $v^{-0.5}$ law if we exclude the results for $Q = 0.43$ L/min what agrees with an analytical model. However, this was not the situation for turbulent flows, where the relationship follows a law which differed from the theoretical $v^{-0.8}$. Higher n values for v^{-n} law were obtained: $n = 1.2$ for T_1 sensor and $n = 1.5$ for the two others.

Figs. 8 and 9 show model results for the same flow rates. For laminar flows (Fig. 8) the curves predict qualitatively the

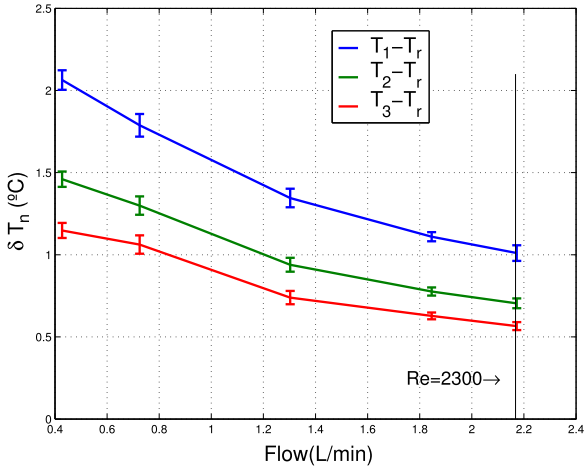

Fig. 6. Experimental results. Laminar flow.

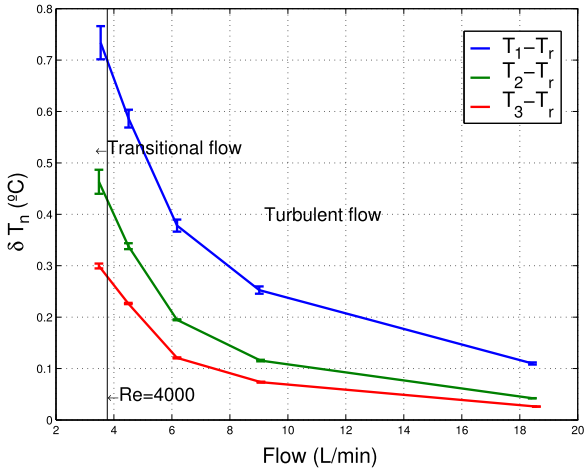

Fig. 7. Experimental results. Non-laminar flow.

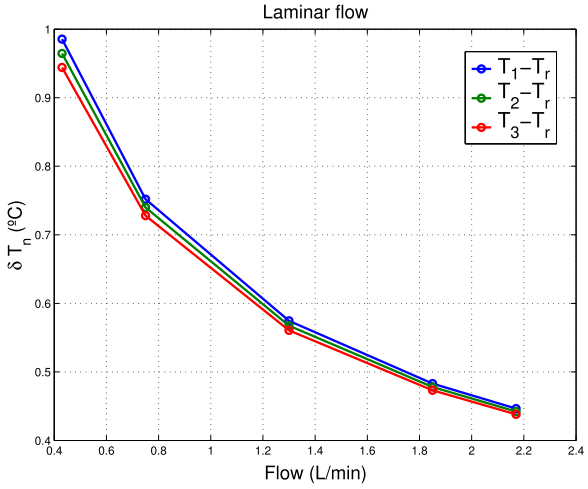

Fig. 8. Model results. Laminar flow.

temperature dependency on velocity. There was no match in quantitative temperature values which also happens in other models shown in the literature [18,17]. This is because many assumptions were carried out to reduce the complexity of the heat transport phenomena and obtain a simple differential equation. For example, Eq. (7) is based on the fact the fluid velocity profile is flat when it reaches a heated plate. Obviously this is not the

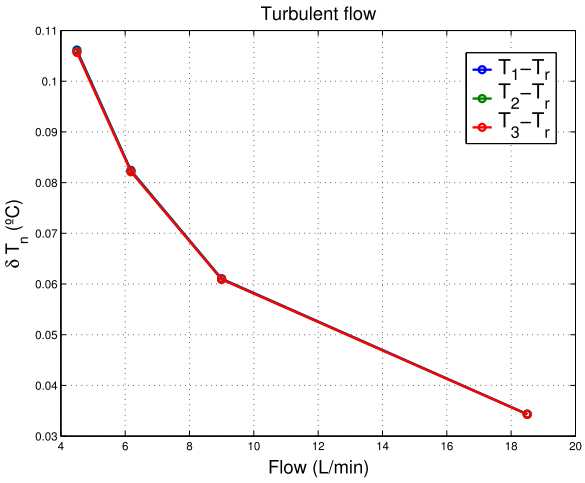

Fig. 9. Model results. Turbulent flow.

situation in the proposal flowmeter. In laminar flows, the velocity profile inside the pipe is parabolic, where the velocity at the axial position is twice the mean velocity. So, it would have been more appropriate to consider that the velocity v used in Eq. (7) was higher. This would have led to obtain a velocity boundary layer narrower and higher temperature values at the position of the downstream sensors.

Another important issue is the fact of heat conduction in the interface between heater and fluid. We assumed that the heat was produced inside the fluid which is flowing with a constant velocity. In fact, the velocity profile is not constant, changing from zero, at the plane position (sensor probe), to higher values as the distance between the flow lines and the plane increases. At the surface of the heater, the heat conduction is dominant whereas a little further away from the heater advection is dominant. In the proposal model, advection is dominant for almost all fluid velocities. This partially explains why the model can show very small differences among the temperature at downstream sensor positions. Even at higher mean velocities these differences are much more negligible, what it is the case of turbulent flows (Fig. 9). Other assumptions like the heat flow in the z-direction is negligible or using an average height of the thermal boundary layer could hide the temperature decrement along the x-axis as well.

A better estimation might be obtained by FEA simulation, but this approach is out of the scope of this work.

5.1. Flow estimation by redundancy

Table 2 shows the confidence interval of estimated flow $\hat{Q}$ and the percentage error computed as follows. From Figs. 6 and 7 and each downstream sensor we obtained a linear piecewise function $\delta T_n(Q)$ containing 10 flows with their corresponding $\overline{\delta T_n}$ output values and interpolation lines among them. Then, we inverted such function to obtain a new one, $Q(\delta T_n)$, wherein δT_n is now the input and the flow, Q, the output. For each experimental δT_n, we get an estimation of flow $\hat{Q}$ which, in turn, is compared with the true flow value to evaluate the error. A total of 25 flow estimations for one true flow value are used to calculate the standard deviation, and with that, the confidence interval assuming that they followed a Gauss distribution. Percentage error is 50-times the confidence interval divided by the true flow.

As the flowmeter makes three estimations of flow at the same time (one per each downstream sensor), they can be averaged to make a result with higher accuracy and whose error is given by Eq. (20), in where S_i is the measurement error of sensor T_i. The rightmost column of Table 2 shows these results.

$$S_{red} = \frac{1}{3}\sqrt{\sum_{n=1}^{3} S_n^2} \tag{20}$$

Table 2 also shows the full scale error for each temperature sensor individually, and using redundancy. Notice the full scale error drops to 0.7%FS. Comparing measurement errors in turbulent and laminar flows, the flowmeter commits bigger errors in laminar flows (6.46% in average) than in turbulent ones (3.44%).

6. Practical considerations for flowmeter implementation

6.1. Operation mode

The flowmeter has three states: inactive, warm-up and measurement (see Fig. 10). In measurement state, all the channels are sampled at 800 Hz, stored using an 800-sample data window and averaged as soon as the channel buffer is full. Hence, four measurements every second are obtained: three differential temperatures, δT_n and the fluid temperature, T_f, which corrects differential temperatures and reduces errors in the following stages of processing. The corrected δT_n are inputs of the calibration curves, $Q_n(\delta T_n)$, whose outputs give three flow estimations. Finally, those outputs are combined into one flow estimation with a more

Table 2
Experimental errors.

Test conditions		$\hat{Q}(\frac{L}{\min})$			Error (%)			
$Q(\frac{L}{\min})$	*Re*	1	2	3	1	2	3	Redundancy
0.43	455	[0.39 0.46]	[0.33 0.53]	[0.37 0.48]	8.29	22.9	12.7	9.2
0.75	771	[0.67 0.82]	[0.66 0.83]	[0.67 0.83]	10.3	11.4	10.9	6.3
1.30	1382	[1.20 1.39]	[1.17 1.43]	[1.16 1.44]	7.2	10	11.1	5.5
1.85	1962	[1.73 1.97]	[1.67 2.02]	[1.69 2.00]	6.52	9.65	8.44	4.8
2.17	2306	[1.91 2.43]	[1.93 2.40]	[1.92 2.41]	11.9	10.9	11.1	6.5
3.54	3739	[2.97 4.10]	[3.18 3.89]	[3.36 3.71]	16	10	4.9	6.5
4.50	4803	[3.86 5.14]	[4.16 4.83]	[4.26 4.74]	14.2	7.4	5.4	5.6
6.18	6561	[5.89 6.47]	[6.01 6.35]	[6.04 6.32]	4.7	2.8	2.3	2
9	9654	[8.50 9.50]	[8.74 9.25]	[8.53 9.47]	5.6	2.8	5.2	2.7
18.5	18,745	[18.32 18.69]	[18.43 18.57]	[18.41 18.59]	1	0.4	0.5	0.4
			Average error (%)		8.57	8.83	7.25	4.95
			FS error (%)		1.5	1	1	**0.7**

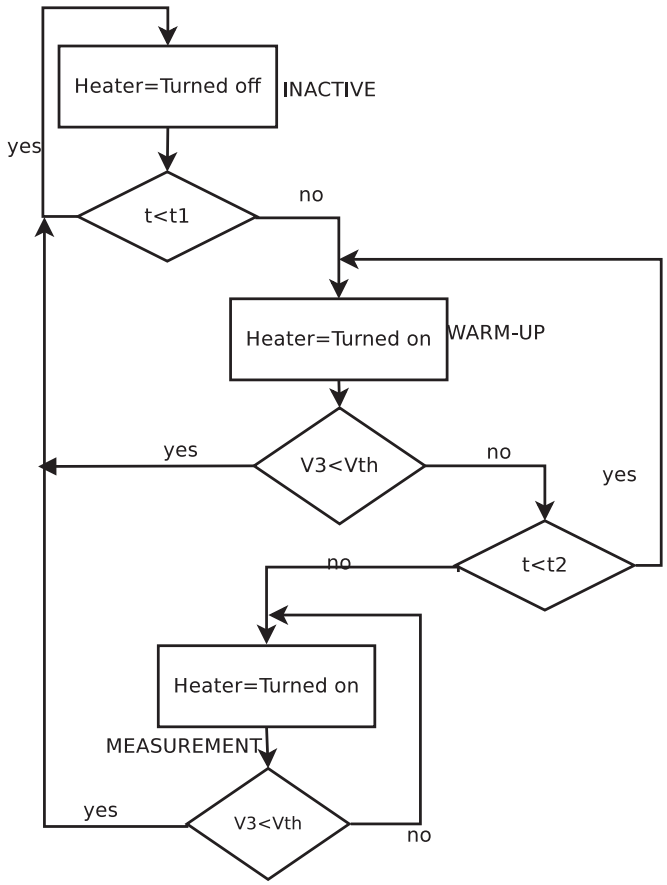

Fig. 10. Operation mode of the flowmeter. Three main states: Measurement, Warm-up and Inactive are shown. The Warm-up state guarantees the signals to be in steady state before the flowmeter starts measuring. Zero-flow and empty pipe conditions can move the flowmeter to the inactive state to prevent the sensor from damage.

reduced error. Redundancy might be also potentially used as an indicator of the quality of the measurement through the variance.

In the inactive state, the flowmeter does not make any flow estimation and in it the calibration process must be carried out. After calibration the heater must be turned on but before starting estimating the flow (Active state), the flowmeter should wait for the signals V_n to get to a steady state. This is the warm-up period, which lasts t_2 seconds.

If the heater is turned on, the voltage V_3 is continuously compared with a threshold V_{th} which prevents the probe from being damaged. This will be explained in the following section.

6.2. Empty pipe and zero-flow detection

Measurement or warm-up states must be interrupted if the pipe is emptied or the fluid stops flowing. The detection of such conditions should turn off the heater and move the system to the inactive state, staying in there for t_1 seconds. This period of time guarantees the probe to reach the starting situation in which the temperature of the downstream sensors is similar to the environmental one. Fig. 10 graphically describes this operation mode. Those situations are easily detected from V_n signals because they show a sudden drop crossing the baseline (see Fig. 11). Asymmetries in the placement of temperature sensors with respect to heater make at least one signal (V_3) keeping below a threshold V_{th} for a long time even though the heater keeps powering the whole medium.

Once the heater is turned off and the process has gone to the

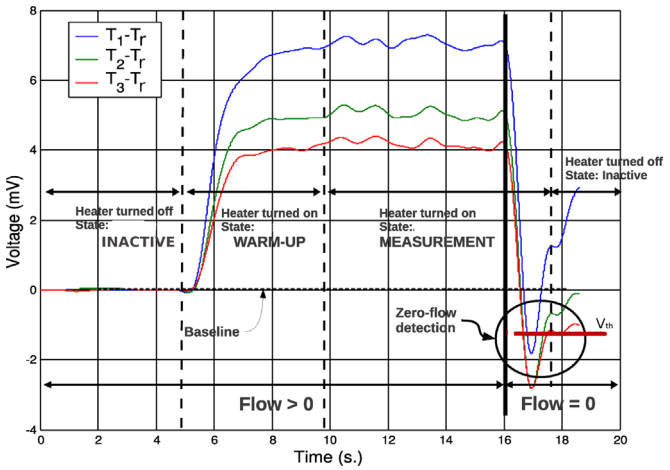

Fig. 11. Zero-flow detection and heater turning on and off procedure. After turning the heater on, the circuit goes into warm-up phase, waiting for the signal to reach the steady state. If V_3 signal becomes lower than the threshold V_{th}, the zero-flow condition or empty pipe condition is detected and the heater is turned off.

inactive state, the flowmeter must detect if there is flow again to go back to the measurement state. This is carried on in warm-up state where the heater is powered again. A decrement in V_3 signal suggests the flowmeter going back to the inactive state and turning the heater off again for a while (t_1 seconds). However, an increment in all V_n signals suggests passing to measurement active state (after t_2 seconds) and keeping turning the heater on.

7. Conclusions

This work shows an electronic device and a theoretical model of an insertion flowmeter based on the calorimetric principle. The flow is measured without using any kind of laminar or bypass elements and it has been tested for laminar, transitional and turbulent flow patterns. It is made up of four temperature sensors and a heater among them. Three of these rtd-type sensors are placed downstream, whereas the fourth one is placed upstream and its function is twofold. On one hand it serves as the reference temperature, T_r for the downstream sensor, T_n ($n=1,2,3$) and, on the other hand, to measure the fluid temperature, T_f. Three differential temperature measurements are sampled per second, $\delta T_n = T_n - T_r$ plus the fluid temperature T_f, which serves to adjust the differential measurements and reduce errors. The meter accuracy is increased by combining the flow estimations given by three downstream sensors (redundancy of measurements). Experimental results make the accuracy rate of the instrument equal to $\pm 0.7\%$ FS in a range between 0.5 L/min and 19 L/min, which is not a usual range for thermal flowmeters in liquids.

The model qualitatively describes the relationship between temperature and mean velocity only in laminar flows but fails to predict the same relationship in turbulent flows or the dependency on the position of the sensors, requiring further research.

This work shows a procedure to measure, warm-up and prevent the probe from damaging in practical implementations when the pipe is emptied or in zero-flow condition based on the positional asymmetries of the outermost sensors (T_3 and T_r) with respect to the heater.

Conflict of interest

There is no conflict of interest.

Acknowledgements

We would like to thank the anonymous reviewers for their comments and suggestions. Following the suggestions, we included several improvements in this paper.

This research has been sponsored by the FEDER project number 1FD97-0375.

Appendix A

Experimental conditions and physical parameters. Tables 3 and 4.

Table 3
Physical properties of the fluid and substrate.

Density	ρ	1	
Heat capacity		1	J/gr K
Dynamic viscosity	μ	0.01	gr/cm s
Thermal conductivity	K	0.58×10^{-2}	W/cm K
Prandtl's number	Pr	7	
FR4 thermal conductivity		0.29×10^{-2}	W/cm K

Table 4
Geometrical values

Heater half length	L	1	cm
Heater width	w	1.32	cm
FR4 height		0.21	cm
T_1 position		2	cm
T_2 position		3	cm
T_3 position		3	cm
T_r position		-3	cm
Heater from border	ξ	3	cm

References

[1] M. Elwenspoek, Thermal flow micro sensors, vol. 2, 1999, pp. 423–435. http://dx.doi.org/10.1109/SMICND.1999.810580.
[2] N.T. Nguyen, Micromachined flow sensors—a review, Flow Meas. Instrum. 8 (1) (1997) 7–16, http://dx.doi.org/10.1016/S0955-5986(97)00019-8.
[3] Y. Zhu, B. Chen, M. Qin, Q.-A. Huang, 2-d micromachined thermal wind sensors 2014, a review, IEEE Internet Things J. 1 (3) (2014) 216–232, http://dx.doi.org/10.1109/JIOT.2014.2319296.
[4] R.-Y. Que, R. Zhu, A compact flexible thermal flow sensor for detecting two-dimensional flow vector, IEEE Sens. J. 15 (3) (2015) 1931–1936, http://dx.doi.org/10.1109/JSEN.2014.2367017.
[5] K. Palmer, J. Jonsson, H. Nguyen, G. Thornell, 2-d thermal velocity sensor for submersible navigation and minute flow measurements, IEEE Sens. J. 13 (1) (2013) 359–370, http://dx.doi.org/10.1109/JSEN.2012.2216866.
[6] O. Sazhin, Novel mass air flow meter for automobile industry based on thermal flow microsensor. I. Analytical model and microsensor, Flow Meas. Instrum. 30 (2013) 60–65, http://dx.doi.org/10.1016/j.flowmeasinst.2013.01.006.
[7] O. Sazhin, Novel mass air flow meter for automobile industry based on thermal flow microsensor. II. Flow meter, test procedures and results, Flow Meas. Instrum. 35 (2014) 48–54, http://dx.doi.org/10.1016/j.flowmeasinst.2013.11.004.
[8] S. Dalola, S. Cerimovic, F. Kohl, R. Beigelbeck, J. Schalko, V. Ferrari, D. Marioli, F. Keplinger, T. Sauter, Mems thermal flow sensor with smart electronic interface circuit, IEEE Sens. J. 12 (12) (2012) 3318–3328, http://dx.doi.org/10.1109/JSEN.2012.2219619.
[9] N.-T. Nguyen, A novel thermal sensor concept for flow direction and flow velocity, IEEE Sens. J. 5 (6) (2005) 1224–1234.
[10] E. Meng, P.-Y. Li, Y.-C. Tai, A biocompatible parylene thermal flow sensing array, Sens. Actuat. A: Phys. 144 (1) (2008) 18–28, http://dx.doi.org/10.1016/j.sna.2007.12.010.
[11] M. Ashauer, H. Glosch, F. Hedrich, N. Hey, H. Sandmaier, W. Lang, Thermal flow sensor for liquids and gases based on combinations of two principles, Sens. Actuat. A: Phys. 73 (1–2) (1999) 7–13, http://dx.doi.org/10.1016/S0924-4247(98)00248-9.
[12] S. Wu, Q. Lin, Y. Yuen, Y.-C. Tai, Mems flow sensors for nano-fluidic applications, Sens. Actuat. A: Phys. 89 (1-2) (2001) 152–158, http://dx.doi.org/10.1016/S0924-4247(00)00541-0.
[13] A. Petropoulos, G. Kaltsas, Study and evaluation of a PCB-MEMS liquid microflow sensor, Sensors 10 (10) (2010) 8981, http://dx.doi.org/10.3390/s101008981.
[14] N.T. Nguyen, R. Kiehnscherf, Low-cost silicon sensors for mass flow measurement of liquids and gases, Sens. Actuat. A: Phys. 49 (1–2) (1995) 17–20, http://dx.doi.org/10.1016/0924-4247(95)01016-T.
[15] O. Aleksić, M.V. Nikolić, M.D. Luković, S.O. Aleksić, P. Nikolić, Analysis and optimization of a thermal sensor system for measuring water flow, Sens. Actuat. A: Phys. 201 (2014) 371–376, http://dx.doi.org/10.1016/j.sna.2013.07.035.
[16] M. Nikolic, B. Radojcic, O. Aleksic, M. Lukovic, P. Nikolic, A thermal sensor for water using self-heated ntc thick-film segmented thermistors, IEEE Sens. J. 11 (8) (2011) 1640–1645, http://dx.doi.org/10.1109/JSEN.2010.2103309.
[17] T.S.J. Lammerink, N.R. Tas, M. Elwenspoek, J.H.J. Fluitman, Micro-liquid flow sensor, Sens. Actuat. A: Phys. 3738 (0) (1993) 45–50, http://dx.doi.org/10.1016/0924-4247(93)80010-E.
[18] N. Nguyen, W. Dtzel, Asymmetrical locations of heaters and sensors relative to each other using heater arrays: a novel method for designing multi-range electrocaloric mass-flow sensors, Sens. Actuat. A: Phys. 62(1–3) (1997) 506–512 (Proceedings of Eurosensors X). http://dx.doi.org/10.1016/S0924-4247(97)01529-X.
[19] A.J. Molina, F. Biscarri, A. Gómez, M.A. Leal, Caudalímetro térmico para líquidos', Oficina Española de Patentes y Marca (Patent number = P201201265).
[20] H. Stachowiak, S. Lassue, A. Dubernard, E. Gaviot, A thermoelectric sensor for fluid flow measurement. Principles, calibration and solution for self temperature compensation, Flow Meas. Instrum. 9 (3) (1998) 135–141, http://dx.doi.org/10.1016/S0955-5986(98)00025-9.
[21] C. Sosna, R. Buchner, W. Lang, A temperature compensation circuit for thermal flow sensors operated in constant-temperature-difference mode, IEEE Trans. Instrum. Meas. 59 (6) (2010) 1715–1721, http://dx.doi.org/10.1109/TIM.2009.2025988.

Alberto J. Molina was born in Lucena (Córdoba) in 1967. He received the B.S. in Physics with intensification in electronics, in Seville in 1990 and Ph.D. degree from University of Seville, in 2010. He has been working as a professor in University of Seville since 1990. He is an author in five books, more than 20 articles, holds three inventions and took part in more than 10 projects. His research interests include signal processing, sensors and the development of new devices or techniques for helping people to access a computer.

Félix Biscarri received the B.Sc. degree in electronic physics and the Ph.D. degree in computer science from the University of Seville, Spain, in 1991 and 2001, respectively. He is currently a Coordinator Professor of Power Electronic with the Polytechnic University School of Seville. His research areas include electricity markets, fault and fraud detection in the power electric industry.

Miguel Ángel Leal received the M.Sc. degree in 2009 from University of Seville (Spain), where he is currently pursuing the Ph.D. degree. He has been working as a professor in University of Seville since 2000. His research interest includes electronics measurement system, industrial control and computational intelligence.

Manuel Merino was born in Seville, Spain, in 1983. He received the Master's degree in computer engineering from University of Seville, Seville, Spain, in 2010, where he has been working toward Ph.D. degree in TAIS research group (Technologies for Care, Inclusion and Health), at the Department of Electronic Technology. His research interests include sensors, biomedical signal processing, affective computing, human computer interface, augmentative and alternative communication, and assistive technology.